Rotational dynamics and aging in a magnetic colloidal glass

E. Wandersman,* V. Dupuis, E. Dubois, and R. Perzynski†
Laboratoire PECSA, UPMC-CNRS-ESPCI, UMR 7195, 4 Place Jussieu, Case 51, 75252 Paris Cedex 05, France
(Received 5 March 2009; revised manuscript received 10 July 2009; published 21 October 2009)

We follow here the freezing of the orientational degrees of freedom of strongly interacting magnetic and charged nanoparticles, as the colloidal glass transition is approached. Using a magnetoinduced birefringence technique, we show that the rotational dynamics drastically slows down following a Vogel-Fulcher law. More precisely, this slowing down occurs above a volume fraction threshold ϕ^*, the value of which depends on the range of electrostatic repulsion between nanoparticles. An interpretation in terms of effective spheres, slightly anisotropic, is proposed. The aging of the rotational dynamics of the more concentrated samples is reported on long time scales, with an exponential growth of the rotational characteristic time with the age t_w of the sample. An attempt of age rescaling at different volume fractions leads us to introduce a ϕ-dependent "birth age" $t_w^0(\phi)$, which diverges analytically at the Vogel-Fulcher volume fraction.

DOI: 10.1103/PhysRevE.80.041504 PACS number(s): 64.70.pv, 71.55.Jv, 45.20.dc, 61.20.Lc

I. INTRODUCTION

In a wide sort of disordered materials, the fluid-solid transition breaks the ergodicity, leading to an amorphous glassy state, out of the thermodynamical equilibrium. Approaching this glass transition, the dynamics of the system drastically slow down and aging processes are encountered. This field of research is presently very active, because numerous questions about the physical nature of the glass transition are still open. The universal character of the glass transition, the physical origin of the slowing down and a scaling interpretation of aging are, for example, points that need to be further explored.

Several conceptual and theoretical advances have extended the degree of universality of the glass transition: the Mode Coupling Theory (MCT) [1] predicts both in molecular and colloidal glasses a divergent relaxation time at a critical temperature (for molecular systems) or a volume fraction (for colloidal glasses). The concept of "jamming" [2] has extended the glass transition to granular matter and to sheared soft matter. Moreover, formal analogies between spin glasses dynamical equations and MCT ones have been revealed [3]. However, even inside the "soft glass family" (colloidal glasses, gels, micellar systems…) some dynamical differences do emerge [4,5]. The diversity of interaction potential between particles in soft systems (being attractive in gels or repulsive in glasses) could be an argument for these discrepancies.

The origin of the slowing down accompanying the glass transition is widely debated and has been recently related to the growth of dynamically correlated domains imposing slow and heterogeneous relaxations in the system [6]. Experimentally, soft glasses are suitable systems (thanks to the size of their elements) to study the nature of the glass transition dynamics, using light scattering technique [7] or confocal microscopy [8]. Heterogeneous and slow dynamics have been reported, both in gels [9] and repulsive glasses [10–12]. However, these results only concern the translational dynamics of the particles. Whereas rotational dynamics of molecular glasses has been well explored (using, for example, dielectric relaxation techniques [13,14]), only scarce results concern the rotational freezing of colloidal glasses or gels [15]. On the theoretical side, the origin of the freezing of the rotational dynamics is always unsurprisingly linked to a strong anisotropy of the interaction potential [16,17]. However, recent results of MCT for a nearly spherical particle dispersed in an isotropic glass of hard spheres [18,19] have extended this problem: the rate of anisotropy has to be incorporated in the rotational dynamics.

As glassy systems are out of thermodynamical equilibrium and present slow relaxation times, their physical properties strongly depend on the elapsed time since they have overpassed the glass transition. They age. An important goal is to find a temporal scale invariance allowing to describe dynamical properties of the systems at any age. Such a rescaling has been done, for example, in spin glasses [20], where a power-law rescaling has been proposed. However, the interesting question of age scaling in other disordered systems is not clear yet [21]. Indeed, in soft glasses, experimental results are controversial: for the translational dynamics, there are some discrepancies between the different experiments performed [5]. For its part, the rotational aging in colloidal glasses is almost absent of recent investigations.

We focus here on these questions, organizing the paper as follows: in the first part, we shall present the dispersions of magnetic nanocolloids (also called ferrofluids). We shall see that ferrofluids are indeed singular systems to study the universal character of the glass transition. In the second part, we show that the original magneto-optical properties of the ferrofluids allow to study the rotational dynamics of the nanoparticles along the colloidal fluid-solid transition. In the third part, the long-time aging of the rotational dynamics and its associated rescaling are presented for different volume fractions. The paper then ends on a discussion of these results emphasizing the specificities of rotational dynamics and the influence of the interparticle interaction potential and its anisotropy. Finally, the introduction of an effective age depending on the volume fraction is discussed.

*Present address: Kamerlingh Onnes Lab, Universiteit Leiden, Postbus 9504, 2300RA Leiden, The Netherlands.
†regine.perzynski@upmc.fr

TABLE I. Properties of the ferrofluid nanoparticles used in this study. The diameter $d=exp[<ln(D)>]$ and the size polydispersity σ are extracted from magnetization measurements adjustment with a lognormal distribution of diameters D. δn_0 is the mean optical anisotropy of the nanoparticles.

Nanoparticles	d (nm)	σ	δn_0
A	9.5	0.35	0.14
B	7	0.3	0.11
C	9	0.28	x

II. FERROFLUID'S PROPERTIES

A. Synthesis and phase diagram

The studied ionic ferrofluids are stable dispersions of magnetic nanoparticles, chemically synthesized in the laboratory following Massart' s procedure (for general properties of the ferrofluids, see [22]). In the present work, we report results on dispersions of maghemite nanoparticles, with a mean diameter $d\sim 10$ nm, electrostatically stabilized thanks to the adsorption of charged citrate species on their surface. The nanoparticles are ferrimagnetic nanocrystals of size smaller than Bloch's Walls and can thus be considered as magnetic monodomains bearing an important magnetic moment $\vec{\mu}$. Its modulus $|\vec{\mu}|$ is here on the order of $10^4\mu_B = m_s V$, where m_s is the saturation magnetization of a nanoparticle, V the volume of the nanoparticle.

In the infinite dilution limit, such a ferrofluid can be seen as a dispersion of noninteracting nanoparticles, statistically independent. From the magnetic point of view, the dispersion is composed of non interacting magnetic moments and is paramagnetic: in the absence of external magnetic field, the whole dispersion has a null magnetization. When a magnetic field is applied, the magnetization of the dispersion follows a Langevin's law. As the magnetic moment of a nanoparticle is proportional to its volume, the fit of the magnetization by a Langevin's law weighted by a log-normal distribution of diameters is a way to determine the nanoparticle size distribution of the ferrofluid [22]. The mean diameter and the size polydispersity of the nanoparticles in our samples are determined in this way and are reported in Table I.

If one increases the volume fraction of nanoparticles in the dispersion, the interaction between nanoparticles is no longer negligible and is rather complex, being composed of (i) Van der Waals attraction, (ii) electrostatic repulsion, that can be screened by the presence of free ions in the solution, and (iii) anisotropic magnetic dipolar interaction. However, a chemical control of the dispersion allows increasing the weight of electrostatic repulsion with respect to the other interactions leading to a Yukawa-like repulsive interparticle potential [23], as in the general case of charged colloids. Previous studies have shown that imposing an ionic strength (screening the electrostatic repulsions) and an osmotic pressure Π in the dispersion determines an equilibrium state with a given volume fraction ϕ. This is experimentally performed by using an osmotic compression technique : the ferrofluid is put in a dialysis bag (Spectrapore, 12–14 kDa), which membrane can be crossed by the smallest molecules (water, ions) but not by the largest ones (nanoparticles, polymers). The osmotic pressure is then imposed by the mass concentration of polymers (dextran, $M=500$ kg·mol^{-1}, Amersham Bioscience) dispersed in the external bath, the ionic strength being imposed independently by the concentration of the electrolyte (here the free trisodium citrate ions [cit]). The duration of the osmotic compression is fixed at three weeks, after which the thermodynamical equilibrium is reached for fluid samples. After this period, the volume fraction is determined by the chemical titration of iron in a known volume of ferrofluid. This protocol is maintained for highly concentrated ferrofluids for which thermodynamical equilibrium is hardly definable or reachable. Note however that for very concentrated ferrofluids, the high viscosity of the sample excludes this method. Then, a density measurement must be used to determine the volume fraction.

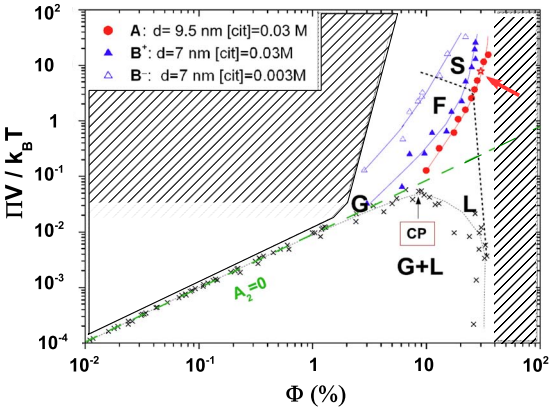

FIG. 1. (Color online) Colloidal phase diagram in the osmotic pressure-volume fraction plane. Phases (G)=gas; (L)=liquid; (F)=fluid; (S)=solid. Crosses indicate the coexistence curve. The box (CP) and the arrow indicate the critical point. Dotted black lines are guides for the eyes delimiting different phases. The green dashed line is the "perfect gas" line, corresponding to a null value of the second virial coefficient A_2. Red circles and blue triangles (open and full) are samples used in this work. Their properties are detailed in the legend. Full lines are guide for the eyes at constant citrate concentration [cit]. The star indicated by an arrow corresponds to a glassy ferrofluid, the translational dynamics of which was extensively studied in our previous studies (Refs. [10,25]).

A "$P-V$-like" colloidal phase diagram of the system has been built up in the $\Pi-\phi$ plane as reproduced in Fig. 1. First, let us remark that this diagram can be divided in two parts by the "perfect gas" $\Pi V=\phi k_B T$ line, where V is the volume of the nanoparticle. In the upper part of the diagram, the global interparticle potential is repulsive whereas in the lower part it is attractive. Secondly, the reported phase behaviors of the ferrofluids in the $\Pi-\phi$ plane reveal strong analogies with molecular systems: (i) a demixion is observed at low volume fractions with a liquid-gas transition and a critical point at the maximum of the coexistence curve [23]. (ii) At high volume fraction, a macroscopic fluid-solid transition is observed at which various macroscopical aspects are reported [24]. Ferrofluids used in the present work are all in the repulsive part of the colloidal phase diagram, but variations in the strength of the interparticle repulsions are considered.

At high volume fractions, the samples are macroscopically solids. However, as shown in [24], their local static structure, determined by Small Angle Neutron Scattering (SANS), reveals the absence of long range order in the dispersion. Indeed, the size polydispersity of the nanoparticles avoids any crystallization process and a fluid-like structure is observed whatever the value of the volume fraction. Moreover, even for highly concentrated ferrofluids, the shape of the static structure factors is typically that of repulsive glasses and rules out the presence of giant aggregates in the dispersion.

Because of their strong analogies with molecular systems, the concentrated ferrofluids are exemplary colloidal glasses. Furthermore, as in these colloidal glasses the particles are nanometric, ferrofluids extend the study of the colloidal glass transition, from micronic down to nanometric lengthscales. Last their chemical control allows a tuning of the interparticle interaction and thus permit to target its role on the dynamical slowing down in glass-forming dispersions. Let us see in the next part how the original properties of ferrofluids allow measuring their rotational dynamics.

B. Magnetoinduced birefringence

From an optical point of view, ferrofluids can be considered as either homogeneous or heterogeneous media in regard to the wavelength of the incident radiation. Using visible light, ferrofluids are homogeneous and isotropic media, in the absence of a magnetic field. When an external magnetic field is applied, these dispersions become optically anisotropic, the optical index of the medium being different in the directions parallel or perpendicular to the field. A macroscopic birefringence is then induced by the magnetic field and its value depends on the strength of the field [26]. This macroscopic birefringence has a microscopic origin: each nanoparticle bears an optical uniaxial anisotropy δn_0.

Whereas the precise origin of this microscopic birefringence is presently still unclear (but probably linked to a small shape anisotropy associated to surface effects [26]), it has been shown that the macroscopic birefringence of a repulsive dispersion is created by a mechanical orientation of the optically anisotropic nanoparticles. When a magnetic field is applied, the magnetic moments μ of the nanoparticles tend to align along the direction of the field. It also mechanically aligns the bodies of the nanoparticles along the field, as the orientation of $\vec{\mu}$ is linked to the crystalline axis of the nanoparticle by the anisotropy energy. Indeed, the nanoparticles are dispersed in a liquid matrix and are—in the dilute regime—able to rotate freely in order to minimize their free energy. The equilibrium state in presence of a magnetic field then corresponds to a partial orientation of the nanoparticles and the birefringence measurement is a way to study the orientational degrees of the nanoparticles. More precisely, this magnetoinduced birefringence corresponds to the orientation of the polarization tensor, and an appropriate time correlator of this quantity can be written as

$$C_2(t) = \langle P_2(\vec{e_i}(t) \cdot \vec{e_i}(0)) \rangle, \tag{1}$$

where P_2 is the second Legendre polynom and $\vec{e}_i$ the direction of the optical axis of the i^{th} nanoparticle.

Using an experimental setup fully described elsewhere [27], we are also able to measure the rotational dynamics of the nanoparticles. The sketch of the experiment is the following: a magnetic field of low intensity $H_0 \sim 2$ kAm^{-1} is applied during the time T_p. If T_p is long enough, the partially oriented stationary state is reached and the dispersion carries a static birefringence Δn_0. After T_p, the field is switched off and the birefringence relaxation is recorded. In dilute dispersions, the nanoparticles are independent and relax towards random orientations. The new macroscopically isotropic equilibrium state is reached by brownian rotational diffusion of the nanoparticles. If in addition the ferrofluid is monodisperse, the relaxation of the induced birefringence is exponential with a characteristic time τ_R

$$\Delta n(t) = \Delta n_0 e^{-t/\tau_R} \tag{2}$$

$$\tau_R = \frac{\eta_0 V_h}{k_B T}, \tag{3}$$

with η_0 the viscosity of the solvent and V_h the hydrodynamic volume of the particles. However, the nanoparticles are not monodisperse, and a weighting by the size distribution must be considered. To take in account this effect of the polydispersity, we have used stretched exponential to adjust birefringence relaxations. For the ferrofluid A of polydispersity $\sigma = 0.3$, with the volume fraction $\phi = 1\%$, we have found a rotational time $\tau_R \approx 6$ μs and a stretching exponent $\alpha \approx 0.8$, close to the value $\alpha = 1$ expected for a dilute monodisperse sample.

III. RESULTS

A. Rotational dynamics of concentrated ferrofluids

The rotational dynamics of ferrofluid A, in the volume fraction range 1 %–30 % and with an ionic strength [cit] $= 0.03M$ are studied using the dynamic birefringence technique introduced in Sec. II B. Our experimental protocol is the following:

(i) The experiment is performed right after the ferrofluid extraction from the compression bath, to avoid any aging processes before the measurement. During the experiment the sample is put in an optical cell ($e = 10$ μm). The time elapsed between the cell preparation and the experience is found to be unimportant (up to one day after the cell preparation).

(ii) All experiments described here are performed with the same magnetic field ($H_0 = 2$ kAm^{-1}) leading to a birefringence $\Delta n_0(\phi)$. An increase in the field intensity (80 Am^{-1}–8 kAm^{-1}) has for consequence to raise the birefringence Δn_0 but has no effect on the dynamics, confirming the linearity of the measured response.

(iii) The duration of the magnetic pulse T_p is adjusted to reach a stationary birefringence state (experimental range: 1 ms–2 s). However, this is not possible with the most concentrated ferrofluid ($\phi = 30\%$ for ferrofluid A). In this latter case, the duration of the pulse is fixed to $T_p = 2$ s. The relaxation of induced birefringence (normalized by Δn_0) at different volume fractions and the values of the birefringence Δn_0

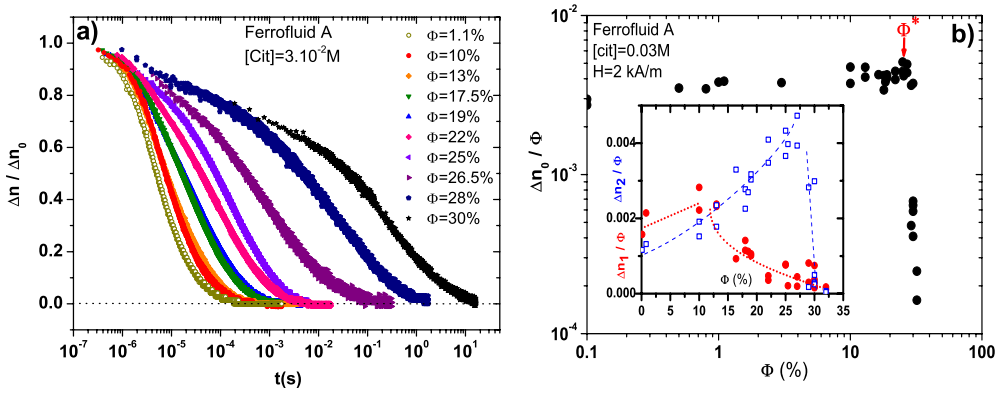

FIG. 2. (Color online) (a) Normalized birefringence relaxations of ferrofluids A at different volume fractions (increasing from left to right). The initial time $t=0$ is defined when the magnetic field is cut off. (b) Normalized birefringence $\Delta n_0/\phi$ for the same magnetic field value $H=2$ kAm^{-1} as a function of the volume fraction ϕ. The value of ϕ^* is indicated by an arrow. Inset : $\Delta n_1/\phi$ and $\Delta n_2/\phi$ as a function of ϕ. Dotted and dashed lines are guides for the eyes.

after the time T_p, normalized by ϕ, are both reported in Fig. 2.

A slowing down of the rotational dynamics is indeed observed in the birefringence relaxations, while increasing the volume fraction. Let's perform a more quantitative analysis:

(i) For dilute ferrofluids, the value of Δn_0 is expected, at the first order, to be proportional to the volume fraction ϕ. Only slight deviations to such a behavior are observed, up to a certain volume fraction ϕ^* above which $\Delta n_0/\phi$ suddenly collapses. This expresses the freezing of the orientational degrees of freedom of the nanoparticles at the experimental time scale. For ferrofluid A with the ionic strength [cit] $=0.03M$, the value found experimentally is $\phi^* \approx 25\%$.

(ii) For dilute ferrofluids, we have previously argued that the magnetoinduced birefringence relaxations are nearly exponential, traducing a brownian rotational dynamics. However, for concentrated ferrofluids, the shape of the relaxations is modified and becomes clearly nonexponential. While increasing the volume fraction, the relaxations become more and more stretched but still keep a short time exponential component. For this reason we fit the relaxations with the following function:

$$\frac{\Delta n(t)}{\Delta n_0} = Ae^{-t/\tau_1} + (1-A)e^{-(t/\tau_2)^{\alpha}}. \tag{4}$$

Inset of Fig. 2 plots the ϕ dependence of the two contributions $\Delta n_1 = A\Delta n_0$ and $\Delta n_2 = (1-A)\Delta n_0$.

(iii) In the fitting process, the short characteristic time τ_1 is set constant to its value at low volume fraction, while the slow contribution is adjusted through the parameters A, τ_2, and α. The evolution of the fit-parameters τ_2 and α with the volume fraction are reported in Fig. 3. If the volume fraction is below ϕ^*, the rotational characteristic time τ_2 only slightly increases, in agreement with numerical simulations performed in reference [28]. On the contrary, for volume fractions larger than ϕ^*, τ_2 drastically raises up (by about four decades in time). An adjustment by the semiempirical Vogel-Fulcher law on the whole concentration range

$$\tau_2(\phi) = \tilde{\tau} e^{\left(\frac{\Psi}{\phi_0 - \phi}\right)}, \tag{5}$$

indicates a divergence of the rotational characteristic time for the volume fraction $\phi_0 = 30 \pm 1\%$. Precisely, for the sample $\phi = 30\%$, no stationary birefringent state can be reached after

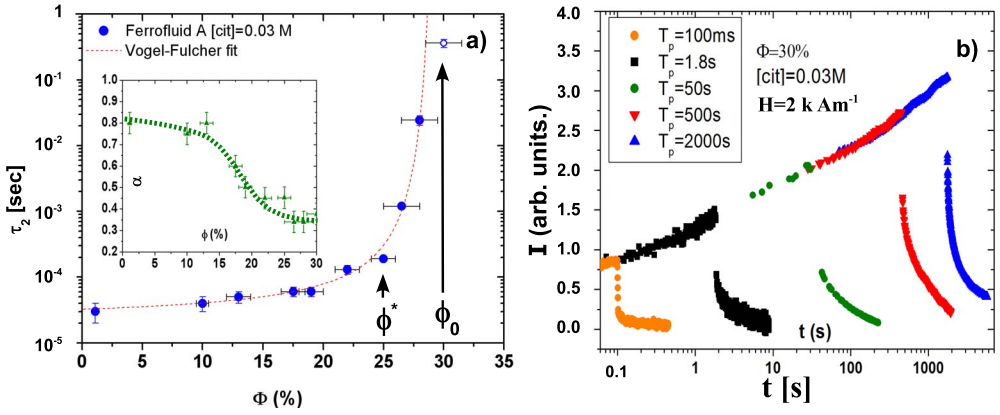

FIG. 3. (Color online) (a) Rotational characteristic time τ_2 extracted from the fit of birefringence relaxations of Fig. 2 as a function of the volume fraction ϕ. The open symbol is the sample at volume fraction $\phi=30\%$ for which no stationary birefringence can be reached after a pulse of magnetic field. The dashed line is a Vogel-Fulcher fit of the data. Inset: Evolution of the stretched exponent α as a function of the volume fraction. The dotted line is a guide for the eye. (b) Increase in the magnetoinduced birefringence for the sample $\phi=30\%$, for the same magnetic field intensity but different values of T_p (increasing from left to right). The initial time $t=0$ is defined when the field is turned on.

TABLE II. Experimental values of the volume fractions ϕ^* obtained for the different ferrofluids A, B^- and B^+ and C, the characteristics of which are indicated (d and [cit]). The characteristic screening length κ^{-1} is calculated from the value of ϕ^* (see the text)

Name	d (nm)	[cit] (mol l^{-1})	ϕ^* (%)	κ^{-1} (nm)
A	9.5	0.03	25 ± 1.5	1.5 ± 0.2
B^+	7	0.03	18 ± 1.5	1.7 ± 0.2
B^-	7	0.003	11 ± 1.5	2.6 ± 0.3
C	9	0.03	22 ± 2	1.7 ± 0.3

any time T_p in our experimental range and the relaxation is strongly dependent on the value of T_p. In Fig. 3(b), the whole pulse is presented for the same value of H_0, but for increasing values of T_p, up to 2000 s. It gives an insight of the raising part of the birefringence signal. Note that in this case the initial time $t=0$ is set at the beginning of the magnetic field pulse [and not at the end as in Fig. 2(a)]. The increase in the birefringence is roughly logarithmic in time, indicating that this sample has a real large characteristic time distribution.

(iv) The variation in the stretching exponent α extracted from the relaxations using Eq. (4) is reported in the insert of Fig. 3(a). Its value is related to the width of the relaxation time distribution. Beginning from the value 0.8 at low volume fractions (due to polydispersity), the stretching exponent sensibly decreases at $\phi=17\%$ ($=0.7\phi^*$), and goes down to the value 0.3, which is reached for very concentrated samples. Such low values of α indicate that the system has an extremely wide distribution of characteristic times, as expected in glass-formers.

(v) For samples of volume fraction larger than ϕ_0, the induced birefringence after T_p is so slow that the signal-to-noise ratio is not acceptable to be presented here. However, a minimal rotational dynamics is still present and is composed of a major short time component and a minor, strongly stretched, long time relaxation [see inset of Fig. 2(b)].

In [24], such a rotational freezing has been already reported with a different ferrofluid (called hereafter ferrofluid B) with a mean diameter ($d=7$ nm) at two different ionic strengths: $B^+([\text{cit}]=0.03M)$ and $B^-([\text{cit}]=0.003M)$. Present results are obtained with ferrofluids A and C (at the ionic strength $[\text{cit}]=0.03M$). Their advantage comes from the larger mean diameter of the nanoparticles ($d \sim 9-9.5$ nm), leading to an increased mean microscopic birefringence δn_0 in regard to dispersions with smaller particles (see Table I) As a consequence, precise measurements can still be performed with concentrated ferrofluids ($\phi > \phi^*$).

We compare in Table II the values of ϕ^* determined for these different ferrofluids.

The value of ϕ^* is found different for the same nanoparticles at two different ionic strengths (B^+ and B^-) [24]. This indicates that the freezing of rotational dynamics in the system depends on the range of the electrostatic repulsion, leading us at the first order to an interpretation in terms of *effective spheres*. Indeed, we may consider that the relevant length in the system is the diameter of a nanoparticle increased by the typical range of the electrostatic repulsion, κ^{-1}

$$\phi_{eff} = (1 + 2\kappa^{-1}/d)^3 \phi. \tag{6}$$

If we make the (simplistic) hypothesis that the rotational freezing at the volume fraction ϕ^* corresponds to the hard-sphere freezing of the effective spheres ($\phi^*_{eff} = \phi_g^{HS} \approx 58\%$), we can evaluate this screening length κ^{-1}

$$\kappa^{-1} = \frac{d}{2}\left(\sqrt[3]{\frac{\phi^*_{eff}}{\phi^*}} - 1 \right). \tag{7}$$

The values of κ^{-1} are reported in Table II. As expected, κ^{-1} is increasing if one decreases the ionic strength (the electrostatic repulsion is in this case less screened). Moreover, we show that for ferrofluids A and B^+ of different nanoparticle diameter but with the same ionic strength, the screening lengths κ^{-1} are well comparable. For $\Phi > \Phi^*$, these effective spheres would then interpenetrate with great difficulty. However, the dynamical freezing of the orientational degrees of freedom observed here for a system of nearly spherical nanocolloids indeed questions the origin of this slowing down. This point will be discussed in Sec. IV A.

Last, we would like to mention the macroscopic aspects of the concentrated ferrofluids. Their ability to flow macroscopically has been checked at different volume fractions. Whereas ferrofluids of volume fraction below ϕ^* are flowing easily macroscopically, the samples become very viscous in the volume fraction range $[\phi^* - \phi_0]$, and hardly flow. For volume fractions above $\phi_0=30\%$, ferrofluids are macroscopically solids and do not flow on a human timescale (years). So, the freezing of the translational dynamics are well comparable to that of the rotational degrees of freedom, as observed with the birefringence technique. The latter is really a helpful witness to spot and analyze the dynamical freezing of the nanoparticles. Note that the freezing of the positional degrees of freedom in a similar ferrofluid has been observed in a Rayleigh Forced Scattering experiment associated to a Soret coefficient determination [29]. Moreover, the study of the translational dynamics has been investigated in [10,25] thanks to X-Ray Photon Correlation Spectroscopy (XPCS) measurements for the ferrofluid A with a volume fraction $\phi=30\%$ and an ionic strength $[\text{cit}]=0.03M$. Slow dynamics and aging associated to the positional degrees of freedom are reported in these papers. We present in the following aging studies of the rotational dynamics in concentrated ferrofluids.

B. Aging of the rotational dynamics in glass-forming ferrofluids

The concentrated ferrofluids studied here are obtained using the osmotic compression technique introduced in Sec. III A. It is during this osmotic compression that the ferrofluids, initially at equilibrium in a fluid state, may be put out of thermodynamical equilibrium. The age of the system will then be counted starting from the time at which the ferrofluid is extracted from the compression bath. We want to notice that another age scale could be introduced by the measurement itself: to perform a birefringence experiment, the

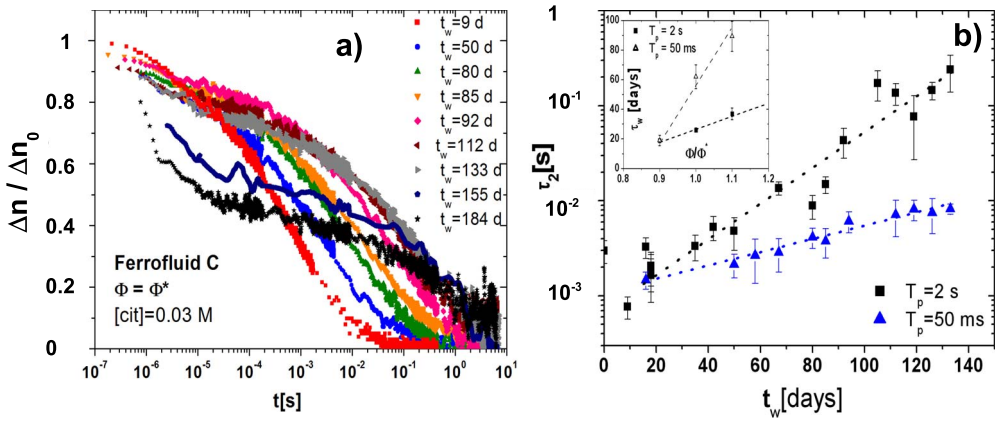

FIG. 4. (Color online) (a) Normalized birefringence relaxations after a pulse of magnetic field of duration $T_p=2$ s, for the ferrofluid C at volume fraction $\phi=\phi^*$ and ionic strength [cit]=0.03M. The different symbols and colors represent different ages t_w of the ferrofluid, counted in days. (b) Rotational characteristic time τ_2 extracted from the previous relaxation as a function of the age of the system at $\phi=\phi^*$ (ferrofluid C). Squares correspond to the pulse duration $T_p=2$ s; Triangles correspond to the pulse duration $T_p=50$ ms. Dotted lines are exponential fits of the data, with characteristic time $\tau_w \approx 26$ days for $T_p=2$ s and $\tau_w \approx 50$ days for $T_p=50$ ms. Inset: characteristic time τ_w as a function of the normalized volume fraction ϕ/ϕ^* for $T_p=2$ s (circles) and $T_p=50$ ms (triangles).

sample is introduced in a thin quartz cell ($e=10$ μm) and thus subjected to a mechanical stress which could induce a slow evolution of the rotational dynamics. However, by opposition to what can be observed for translational dynamics no dependence of the rotational relaxation after an alignment of the nanoparticles by a small field is found in regard to the time elapsed since the cell preparation, for durations as long as one day. As a consequence, only the very long time evolution age t_w counted in day since the extraction of the sample from the compression bath is considered and a new cell is prepared for each measurement.

Aging of the rotational dynamics is studied with ferrofluids A and C, (their characteristics are in Table I). Their rotational dynamics at the ionic strength [cit]=0.03M are analogous, however ϕ^* is close to 22% for ferrofluid C (25% for ferrofluid A). The rotational aging is studied for series of samples at different ϕ for ferrofluid A (the whole volume fraction range is explored but just at few ages) and C (weekly measurements at volume fractions around ϕ^*: $\phi=0.9\phi^*$; $\phi=\phi^*$, $\phi=1.1\phi^*$). The birefringence experiments are proceeded according to the following protocol:

(1) The day and the precise hour (precision of minute) of the cell preparation is collected. The optical transmission of the sample is measured two minutes after the preparation. The first dynamical birefringence experiment is proceeded six minutes after the preparation.

(2) Aging on long time scales (>1 month) is considered. The ferrofluid is kept in a closed bottle filled up with dodecane, impermeable to water (solubility of $H_2O \approx 0.006$ wt [30]), to avoid any variation in the volume fraction and stored away from light to prevent any citrate deterioration. Some chloroform drops (non miscible with the dispersion) are added in the bottle to exclude any bacterial proliferation which is possible at the neutral pH of ionic ferrofluids. These precautions prevent any chemical evolution of the dispersions, the chemical stability of the $\gamma-Fe_2O_3$ nanoparticles being guaranteed by the neutral pH. Moreover we have checked by Small Angle Neutron Scattering [24] over a period of two years: that the form factor of the nanoparticles is preserved while diluting (and sonicating) concentrated samples in water in the same conditions of pH and ionic strength, that no detectable variation in the peak position of the structure factor of concentrated dispersions is observed within the resolution of the experiment.

(3) A new cell is prepared each week and the rotational dynamics of the sample are measured. Reproducibility of the experiments is checked.

(4) The dynamical birefringence experiment measures the response of the system to a pulse of magnetic field, the duration and intensity of which can be tuned. The effect of the variation in these parameters is studied.

The normalized birefringence relaxations at different ages, of the ferrofluid C at the volume fraction $\phi=\phi^*$, are presented in Fig. 4(a), for a pulse duration T_p of 2 seconds. The same experiment is performed with $T_p=50$ ms. In both experiments, a slowing down of the rotational dynamics is observed on long time scales [see Fig. 4(b)]. While the age of the ferrofluid sample increases, the dynamics becomes slower and slower which can be associated to a gradual freezing of the rotational degrees of freedom. For the oldest ages, the birefringence signal Δn_0 is really low, and the relaxation presents a major short time part and a minor long time one. Such a behavior is never observed for ferrofluids with a volume fraction well below ϕ^*.

The characteristic time τ_2 of the birefringence relaxations can be extracted in the same way as in Sec. III A, using a fit of the relaxation by equation (4). The evolution of the characteristic time τ_2 with the age t_w of the dispersion, at $\phi=\phi^*$, is presented in Fig. 4(b), for the two different values of T_p. The characteristic time $\tau_2(\phi^*,T_p,t_w)$ is found to increase exponentially with the age t_w. A fit of this curve is then proposed according to the equation

$$\tau_2(\phi^*,T_p,t_w) = \tau_2(\phi^*,T_p,0)e^{t_w/\tau_w(T_p)}. \quad (8)$$

In this equation $\tau_2(\phi^*,T_p,0)$ represents the characteristic time of the relaxation at zero age. It is a priori T_p dependent,

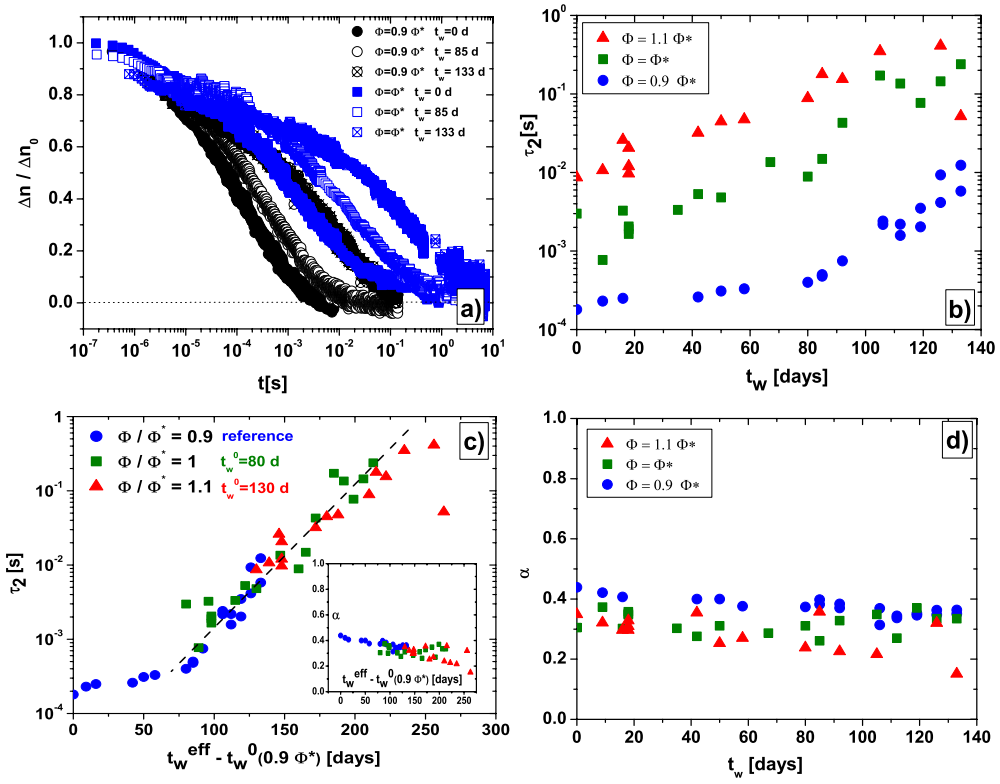

FIG. 5. (Color online) (a) Normalized birefringence relaxations of ferrofluid C at volume fractions $\phi=0.9\phi^*$ and $\phi=\phi^*$, for three different ages t_w and $T_p=2$ s. (b) (c), and (d) Rotational characteristic time τ_2 and stretched exponent α extracted from the relaxations as a function of the age of the system (Ferrofluid C at $\phi=0.9\phi^*$, $\phi=\phi^*$, and $\phi=1.1\phi^*$) plotted as a function of t_w in figures (b) and (d), and as a function of the reduced variable $t_w^{eff}-t_w^0(0.9\phi^*)$ in main figure (c) and its inset.

in our range of T_p, for $\phi \geq \phi^*$. The quantity $\tau_w(T_p)$ is the characteristic time of the exponential evolution of τ_2 as a function of the age t_w which depends on the pulse duration T_p. The values of τ_w extracted from an exponential fit [see Fig. 4(b) and inset of the same figure] are $\tau_w=26\pm2$ days for $T_p=2$ s and $\tau_w=62\pm8$ days for $T_p=50$ ms.

However, the exponential increase in rotational characteristic time, which is observed as the concentrated ferrofluid ages, is associated in Eq. (4) to a stretching exponent α only weakly dependent on age, as it is illustrated in Fig. 5(d).

The same experiment is performed with ferrofluids C at the two other volume fractions, $\phi=0.9\phi^*$ and $\phi=1.1\phi^*$. In all cases the same behavior is observed, namely, with an exponential increase in the rotational characteristic time. Note in the inset of Fig. 4(b) that $\tau_w(T_p=2$ s) is only very weakly dependent on ϕ and that hereafter all the reported experiments are performed with $T_p=2$ s. The relaxation time τ_w is considered, at the first order, as independent on ϕ.

A comparison between the normalized birefringence relaxations of ferrofluid C at volume fractions $\phi=0.9\phi^*$ and $\phi=\phi^*$ at different ages is presented in Fig. 5(a). The shape of the relaxation of the sample at volume fraction $\phi=0.9\phi^*$ for the age $t_w=133$ days is roughly similar to the relaxation of the sample at volume fraction $\phi=\phi^*$ for the age $t_w=0$ day. This is quantified in terms of τ_2 and α in Figs. 5(b) and 5(d) showing that such an equivalence is also observed for samples $\phi=\phi^*$ and $\phi=1.1\phi^*$. There is then an overlap between the relaxation shapes at different volume fractions and different ages. The rotational dynamics of a less concentrated sample slow down as it ages, and from a certain age becomes as slow as the rotational dynamics of a more concentrated sample at young age.

This overlap conducts us to introduce an effective age, which depends on the volume fraction

$$t_w^{eff}(\phi) = t_w + t_w^0(\phi). \tag{9}$$

The parameter $t_w^0(\phi)$, homogeneous to a time, is fixed to zero for volume fractions less than $0.7\phi^*$. Indeed, for volume fractions less than $\phi^*/2$, no aging is ever observed here, the rotational dynamics is age-independent, at the time scale of the experiment. A slight rotational aging is only observed at very long ages for samples at the volume fraction $\phi=0.7\phi^*$, while the more concentrated samples present a strong rotational aging. For these more concentrated samples, $t_w^0(\phi)$ [and thus $t_w^{eff}(\phi)$] is chosen to perform the age rescaling as in Fig. 5(c) (main figure and inset) at different volume fractions.

Figure 6(a) presents for both ferrofluids A and C the reduced variations of $\tau_2/\tau_2(\phi=0)$ as a function of t_w^{eff}. A scaling is obtained at large t_w^{eff} for all our samples, with an exponential growth of the rotational characteristic time with t_w^{eff}.

$$\tau_2(\phi,t_w) = Ae^{t_w^{eff}/\tau_w} = Ae^{t_w/\tau_w}e^{t_w^0(\phi)/\tau_w}. \tag{10}$$

A being a constant, homogeneous to a time. At $t_w=0$ day, this latter equation should be coherent with the experimental

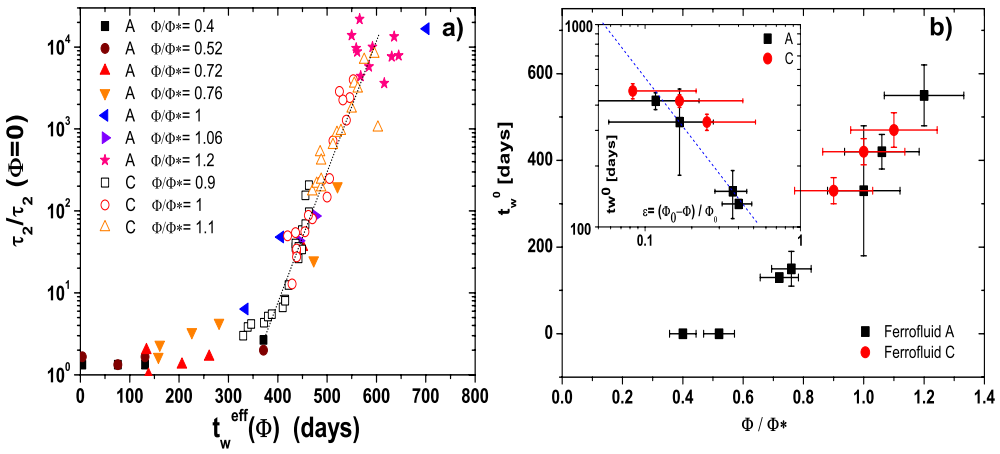

FIG. 6. (Color online) (a) Age rescaling of the rotational characteristic time τ_2 of both ferrofluids A (full squares) and C (open circles) introducing an effective age $t_w^{eff}(\phi)$. The dotted line corresponds to the best fit of expression (10) with $\tau_w \approx 26$ days. (b) Evolution of the lag-age parameter $t_w^0(\phi)$ for ferrofluids A (black squares) and C (red circles) as a function of the reduced volume fraction ϕ/ϕ^*. Inset: $t_w^0(\phi)$ as a function of the reduced parameter ϵ. The blue line has a slope −1 in this log-log representation.

observation of section A, thus with Eq. (5). It imposes the following evolution law for $t_w^0(\phi)$, providing that τ_w is ϕ-independent:

$$t_w^0(\phi) \propto \frac{1}{\phi_0 - \phi}, \tag{11}$$

where $\phi_0 = 1.2\phi^*$, the Vogel-Fulcher volume fraction.

The variation of the parameter $t_w^0(\phi)$ as a function of the normalized volume fraction ϕ/ϕ^* is presented in the Fig. 6(b). The evolution of $t_w^0(\phi)$ as a function of $\epsilon = \frac{\phi_0 - \phi}{\phi_0}$ is reported in the inset. It is rather compatible with the power-law behavior of Eq. (11), meaning that we observe at large t_w^{eff}

$$\tau_2(\phi, t_w) = \tau_2(\phi) e^{t_w/\tau_w}. \tag{12}$$

IV. DISCUSSION

We report in Sec. III a drastic slowing down of the rotational dynamics in concentrated ferrofluids, associated to aging phenomena on long time scales. The aims of the following discussion are double. In the first part, we discuss the origin of the rotational freezing while increasing the volume fraction. Our results will be faced to experimental and theoretical results of the literature concerning the freezing of the orientational degrees of freedom at the glass transition. In the second part, we adopt a phenomenological approach to describe the rotational aging in the concentrated ferrofluids emphasizing that the introduction of an effective age allows to assemble aging of ferrofluids at different volume fractions.

A. Slow rotational dynamics (at $t_w = 0$)

The rotational dynamics of concentrated ferrofluids probed through their magnetoinduced optical properties, is explored in this work. A drastic slowing down of the dynamics is reported here above a volume fraction ϕ^*, which depends both on the size of the particles and on the ionic strength of the dispersion. Let us briefly recall the main features of this slowing down: above ϕ^*, the characteristic rotational time is increasing following a Vogel-Fulcher law, which is usual in glasses, with a divergence at a volume fraction ϕ_0 (for the ferrofluid A, $\phi_0 \approx 30\%$). Moreover, the birefringence relaxations become clearly nonexponential, the decrease in the stretching exponent α being a good indicator of the widening of the rotational characteristic time distribution in glassy samples. Our results concerning the orientational degrees of freedom are then well comparable to generic dynamical features observed at the glass transition, which are usually reported for the positional degrees of freedoms [31].

Indeed, whereas the rotational dynamics has been well explored in molecular glasses (using, for example, dielectric measurements [14,32]), only scarce results concern these degrees of freedom in colloidal glasses. Some experiments using a probe molecule [33] have been performed but have the disadvantage—and the interest—to be sensitive to the relative size of the solvent molecules with respect to the solute (see [33]). Depolarized light scattering experiments (DLS) on *anisotropic* colloids [15] (laponite) have shown slow rotational dynamics with aging. Last, in [34], the rotational dynamics of a spherical colloid which is optically anisotropic, in an isotropic interaction potential, is measured experimentally using DLS and reveals only a slight increase (factor 2 at $\phi \sim 50\%$) of the rotational diffusion coefficient, mainly caused by hydrodynamical frictions. To summarize, no rotational slowing down has ever been experimentally reported for nearly spherical colloids.

On the theoretical side, the origin of the rotational freezing is also unsurprisingly linked to an anisotropy of the interaction potential (which can be due to an anisotropy of shape). In [16], the authors consider a model of orientational glass (model-systems for which positional degrees of freedom are settled) constituted of an ensemble of hard needles (that cannot cross each other) on a cubic lattice. They find that the length of the needle is ruling the glass transition. In [17], the dynamics of a two-dimensional assembly of structureless rotors, interacting via a frustrated anisotropic poten-

tial, is considered. When temperature is decreased, the calculated correlation functions exhibit more and more slow dynamics, and their decrease is two steps like and nonexponential. In [16,17], the main features of the rotational dynamics of glass forming systems match well with these observed in our concentrated ferrofluids. However, in both references, a strong anisotropy is required to observe a rotational freezing at the glass transition.

The Mode Coupling Theory has considered the effect of the rate of anisotropy of a particle on its rotational dynamics in a dense hard sphere environment. Whereas the rotational dynamics of an elongated dumbbell (two fused hard-spheres) dispersed in a hard sphere (isotropic) system follows usual MCT results, the rotational dynamics of a nearly spherical dumbbell is less intuitive [18,19]. In the latter case, called "Weak Steric Hindrance scenario" (WSH), a slowing down of the rotational dynamics and the existence of a nonergodicity plateau are observed for the nearly spherical particle but they are only visible on the even l angular correlators C_l, the angular motion being projected on the spherical harmonics basis

$$C_l(t) = \langle P_l[\vec{e_i}(t) \cdot \vec{e_i}(0)] \rangle, \tag{13}$$

where P_l is the Legendre polynom of order l and $\vec{e}_i$ the direction of the axis of the i^{th} nearly spherical dumbbell.

Referring to these results from literature, an anisotropy inside the system is needed to fully understand the origin of rotational freezing of the concentrated ferrofluids. This led us to investigate the source of anisotropy in our colloidal dispersions. Firstly, the anisotropic magnetic dipolar interaction, could be incriminated. Correlations between the magnetic moments of the nanoparticles at large volume fractions could hinder the rotation of the particle. However, in this case, the dynamics of the magnetic moment should be slow at room temperature. Magnetization measurements of concentrated ferrofluids [35] reveal a paramagnetic behavior at room temperature and exclude this hypothesis, at least for dispersions based on maghemite nanoparticles of diameter $d < 8.5$ nm. As a consequence, the dipolar interaction is not the source of the rotational freezing of the ferrofluid B ($d=7$ nm), but cannot be strictly excluded for the ferrofluid A ($d=10$ nm), for which the magnetic moments are larger (and thus the dipolar magnetic interaction). Magnetic measurements on dispersions of these larger particles are intended to be done in a near future.

Another source of anisotropy could be the shape of the nanoparticles themselves. The microscopic transition electron microscopy (TEM) pictures of the dispersion show that the particles are roughly spherical, albeit being more rock like. This shape imperfection could result in a slight anisotropy. However, we also report here that the rotational dynamics is affected by a variation in the intensity of the electrostatic repulsions (ϕ^* depends on the ionic strength of the dispersion, for ferrofluid B). This indicates that at the glass transition, the rotational freezing of the effective objects, constituted of the nanoparticle plus a layer which typical size is the range of electrostatic repulsions κ^{-1}, have to be considered. The rotational freezing in concentrated ferrofluids must then be related to an anisotropy at the scale of the double layer, which could be induced by the imperfect shape of the particles.

Making the hypothesis that the anisotropy responsible for the rotational freezing is an anisotropy of the effective objects, this anisotropy remains always very low in comparison to the cases considered in [16,17]. Hence, our experimental system is close to the WSH scenario, discussed above, of a slightly anisotropic particle in an interaction potential dominated by electrostatic (isotropic) repulsions. A further step is done remembering that the birefringence properties, as we have mentioned, are related to the orientation of the polarization tensor, a second rank tensor which is, as a consequence, sensitive to the $l=2$ component of the orientational dynamics. With such an angle of view, the rotational freezing observed in concentrated ferrofluids is understandable and is, to our knowledge, the first colloidal system to test the WSH-MCT scenario.

However, the details of the physical mechanism of the slow motion are still unclear. Whereas the existence of dynamical heterogeneities for the translational dynamics is demonstrated in our system [10,12], the birefringence technique, used to probe the rotational dynamics, does not allow to discriminate easily between homogeneous and heterogeneous dynamics. Thus, one may consider two different scenarios. The "homogeneous case" would lie on the assumption that each nanoparticle rotates in an effective medium described by a renormalized viscosity η^{eff}, which takes into account all the frictions forces in the dispersion. The rotational slowing down would be the result of the Vogel-Fulcher divergence of the effective viscosity at high volume fractions

$$\frac{\tau_2}{\tau_1} \sim \frac{\eta^{eff}}{\eta_0} \tag{14}$$

$$\eta^{eff}(\phi) \sim \eta_0 \, exp\left(\frac{\Psi}{\phi_0 - \phi}\right), \tag{15}$$

where η_0 is the solvent viscosity and Ψ a constant without dimension. On the other hand, the "heterogeneous interpretation" assumes that the rotational slowing down is related to dynamically correlated domains of size ξ^{eff}, inside which the rotational dynamics occurs in a cooperative way, in an analogous way with the cooperative translational motions reported in the literature [8,11,36].

Experimentally two processes in the rotational dynamics of our system are distinguished : first, the short-time process characterized by Δn_1 and τ_1, is an individual process and corresponds to the random exploration of the angular cage at short time, as in [16]. Secondly, the long time rotational dynamics, characterized by Δn_2, τ_2, and α, corresponds to collective angular rearrangements of the cages. Considering that the slow cooperative events contribute to the static birefringence Δn_2, whereas the Δn_1 contribution arises from individual motions, the ratio $\Delta n_2 / \Delta n_1$ is thus, in a first approximation, the number of dynamically correlated particles

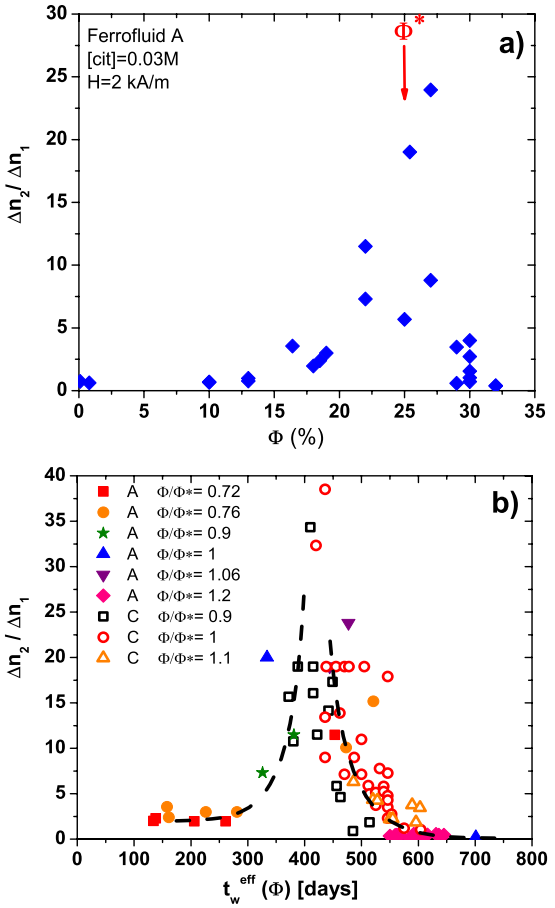

FIG. 7. (Color online) (a) ϕ dependence of the ratio $\Delta n_2/\Delta n_1$, proportional at the first order to the number of nanoparticles collectively involved in the slow dynamics. Measurements performed with ferrofluid A with ages $0<t_w<250$ days. (b) t_w^{eff} dependence of the ratio $\Delta n_2/\Delta n_1$ at various volume fractions. Dashed lines are guides for the eye.

$$\frac{\Delta n_2}{\Delta n_1} \sim \left(\frac{\xi^{eff}(\phi)}{d}\right)^3, \tag{16}$$

times a factor of orientation on the order of 1 up to ϕ^* which is falling down above ϕ^* as $\Delta n_0/\phi$ in Fig. 2(b). The evolution of this ratio with ϕ is plotted on Fig. 7(a). It shows that in the experiment, the collective process emerges above $\phi^*/2$, then dominates in our time window around ϕ^* and finally decreases progressively as it becomes too slow to be observed in the experiment. At the volume fraction ϕ^*, we find $\xi^{eff}\sim 3$ typical nanoparticle diameters, a result in a qualitative agreement with the results concerning the translational dynamics presented in [8,36]. Note that in principle ξ^{eff} may continue to increase above ϕ^*, but that we are not able anymore to quantify it with the ratio $\Delta n_2/\Delta n_1$ in the experiment. Indeed, in ref [11], the authors quantify the cooperativity of the translational dynamics by measuring the dynamical susceptibility χ^* from time resolved photocorrelation spectroscopy [9–11]. A nonmonotonic behavior of $\chi^*(\phi)$ is found while increasing ϕ, with an unexpected drop close to the dynamical arrest volume fraction. This drop is due to the competition between reduced particle displacement at high ϕ, while the dynamical correlation length ξ is still monotonously increasing. Thus, our reported drop of the $\Delta n_2/\Delta n_1$ values at large ϕ could share the same origin. The reduced angular displacement close to ϕ_0 could hinder the growth of a rotational dynamical correlation length in this high ϕ regime.

In supercooled liquids, the Stokes-Einstein relation is violated, this fact being interpreted as a decoupling between the diffusion coefficients and the macroscopic viscosity, due to the presence of these correlated domains [37]. However, considering the birefringence technique as a local probe of the friction forces, the opening question carried by our work is the following: is there a mesoscopic lengthscale on which a "Stokes-Einstein-like" relation can hold? How far would this lengthscale be related to the size of the dynamically correlated domains? Could we write $\eta^{eff}\sim\eta_0(\xi^{eff}/d)^3$? Theoretical answers to these questions could be of interest to understand the origin of these dynamically correlated domains.

B. Aging of the rotational dynamics

The second part of this discussion is devoted to the aging phenomena of the rotational dynamics in concentrated ferrofluids. For ferrofluids the volume fraction of which is well below ϕ^*, no rotational aging is observed. More surprisingly, for highly concentrated samples ($\phi\geq\phi^*$), no rotational aging is observed on timescales similar to those reported for the translational aging ($<10^4$ s) probed by XPCS measurements [25]. This difference between the rotational and the translational aging-timescale may be a sign of the decoupling of these degrees of freedom in our glass-forming ferrofluids. The aging of the rotational dynamics is then investigated here on long timescales ($\sim$1 month). As a unified understanding of aging phenomena occurring in disordered out-of-equilibrium systems remains a challenging question of actual researches on the glass transition [38], a brief overview of aging in different systems can be interesting to begin this discussion:

Standard model systems to study orientational aging are spin-glasses for which, for example, the rescaling of the thermoremanent magnetization (TRM) at different ages has been achieved (see, for example, [20]). However, the physical origin of aging in spin glasses is still under investigation and actual developments are relating it to the growth of a dynamical correlation length [39].

For structural glasses, experimental results on rotational aging are more controversial and their comparison with spin-glass systems, which could extend the degree of universality of aging processes at the glass transition, are not always easy tasks [14,32]. One of the interesting questions on aging in structural glasses is the time scale on which aging occurs in regard to the structural relaxation time and its dependence with the quench temperature. In [40], a simulation of a Lennard-Jones glass is presented. Aging is taking place on timescales longer than the structural relaxation times, after the quench into the glassy state. The observed long time aging scales in a similar way as in spin glasses.

For colloidal systems, aging is also extensively studied, but these works mostly concern the translational dynamics

[7,25]. The reported aging of translational dynamics in colloidal glasses is not trivial and differs sometimes from a system to another [5]. In [25] the aging of translational dynamics in a concentrated ferrofluid (at the volume fraction $\phi_0=30\%$ where the rotational characteristic time diverges) has been considered, using XPCS for ages ranging between 100 s to 10^4 s. At young ages, the evolution of the translational characteristic time is exponential with the age. At older ages, a power-law behavior is observed, in concordance with the spin glass case. Aging of the rotational dynamics in colloidal glasses is quite absent of experimental investigations. To our knowledge the only previous study of rotational aging of glass-forming colloidal dispersions was proposed in [15], using DLS on Laponite. An exponential increase in the rotational characteristic time with the age was reported. However, these results concern anisotropic colloids and no variation in the volume fraction is considered.

In the present study, we observe rotational aging on long timescales, the dynamics becoming slower and slower with the age of the system. Similarly to results reported in [15], the characteristic time of the birefringence relaxation increases exponentially with the age, the form of the birefringence relaxations being also modified (with a short time dynamics component progressively dominating). These last behaviors exclude any simple age rescaling [for example, in $(t/t_w)^{\mu}$, as in spin glasses]. Interestingly, the characteristic time of the aging process, τ_w is dependent on the timescale probed in the experiment, imposed by T_p, meaning that the whole characteristic time distribution is not aging in the same way. However, at large T_p ($T_p=2$ s), the characteristic time of aging τ_w becomes roughly independent on the volume fraction ϕ, meaning that aging is then comparable at close volume fractions. Furthermore, up to a certain age, the rotational dynamics of a ferrofluid at a given volume fraction becomes comparable to the rotational dynamics of a more concentrated sample at zero age. This leads us to introduce an effective age that depends on the volume fraction ϕ, to rescale our results at different ϕ, shifting the relaxation times by a quantity $t_w^0(\phi)$ along the t_w axis. This ϕ-dependent "birth-age" increases as a power law with the volume fraction, a direct consequence of the Vogel-Fulcher variation of τ_2 at zero age.

If we return to the interpretation of the slow dynamics in terms of dynamically correlated domains of size ξ^{eff}, the aging observed imposes to consider the effect of the age t_w. Figure 7(b) plots the ratio $\Delta n_2/\Delta n_1$ as a function of t_w^{eff}. Following expression (16), it gives the number of correlated nanoparticles up to t_w^{eff} on the order of 400–450 days [$\sim t_w^0(\phi^*)$], effective age at which ξ^{eff} reaches ~ 3.3 particle diameters. For larger t_w^{eff}, $\Delta n_2/\Delta n_1$ decreases. However the factor of orientation becoming lower and lower in the experiment, the ratio $\Delta n_2/\Delta n_1$ does not quantifies anymore the number of correlated nanoparticles and the correlation length ξ^{eff} may continue to increase as the system ages.

V. CONCLUSION

Slow rotational dynamics, accompanied by aging on a long time scale, are reported in a repulsive colloidal glass of magnetic nanoparticles. The volume fraction threshold ϕ^* of the rotational slowing down depends on the range of the electrostatic repulsions, leading to an interpretation in terms of freezing of slightly anisotropic effective nanospheres. Above ϕ^*, aging processes are observed, with an exponential growth of the rotational characteristic time with age. To unify the rotational aging of samples at different volume fractions, we introduce a ϕ-dependent effective age $t_w^{eff}(\phi)=t_w+t_w^0(\phi)$. This operation allows to separate, at large t_w^{eff} the contributions of aging and concentration in slow rotational dynamics.

This conjugated effect of age and volume fraction on the dynamics had never been considered in colloidal glasses and points out the peculiar character of the volume fraction as a control parameter of the colloidal glass transition. Indeed, in molecular or magnetic systems, the glass transition is driven by the bath temperature which is an external adjustable thermodynamical quantity. Moreover, in the case of spin glasses, the temperature can be changed during aging. Due to memory or rejuvenation effects, aging at a temperature T is not trivially related to the aging at a close temperature $T-\Delta T$ [41].

Whereas on the experimental side, such temperature-cycling experiment are feasible, a slight variation of ϕ during the aging, cannot be easily achieved. It will be therefore interesting in a future work to use the osmotic pressure as a control parameter. Indeed, during the osmotic compression, the osmotic pressure of the bath can be externally imposed (thus imposing a variation in the volume fraction).

[1] W. Gotze, J. Phys.: Condens. Matter **11**, A1 (1999).
[2] A. Liu and S. Nagel, Nature (London) **396**, 21 (1998).
[3] T. R. Kirkpatrick and P. G. Wolynes, Phys. Rev. B **36**, 8552 (1987).
[4] K. Dawson, Curr. Opin. Colloid Interface Sci. **7**, 218 (2002).
[5] L. Cipelletti and L. Ramos, J. Phys.: Condens. Matter **17**, R253 (2005).
[6] P. Mayer, H. Bissig, L. Berthier, L. Cipelletti, J. P. Garrahan, P. Sollich, and V. Trappe, Phys. Rev. Lett. **93**, 115701 (2004).
[7] L. Ramos and L. Cipelletti, Phys. Rev. Lett. **87**, 245503 (2001).
[8] E. R. Weeks and D. A. Weitz, Phys. Rev. Lett. **89**, 095704 (2002).
[9] A. Duri and L. Cipelletti, EPL **76**, 972 (2006).
[10] E. Wandersman, A. Duri, A. Robert, E. Dubois, V. Dupuis, and R. Perzynski, J. Phys.: Condens. Matter **20**, 155104 (2008).
[11] A. D. P. Ballesta and L. Cipelletti, Nat. Phys. **4**, 550 (2008).
[12] E. Wandersman, Y. Chushkin, A. Robert, E. Dubois, V. Dupuis, and R. Perzynski (unpublished).
[13] M. A. Miller, M. Jimenez-Ruiz, F. J. Bermejo, and N. O. Birge,

Phys. Rev. B **57**, R13977 (1998).
[14] R. L. Leheny and S. R. Nagel, Phys. Rev. B **57**, 5154 (1998).
[15] S. Jabbari-Farouji, E. Eiser, G. H. Wegdam, and D. Bonn, J. Phys.: Condens. Matter **16**, L471 (2004).
[16] C. Renner, H. Lowen, and J. L. Barrat, Phys. Rev. E **52**, 5091 (1995).
[17] S. J. Lee and B. Kim, Phys. Rev. E **60**, 1503 (1999).
[18] S.-H. Chong, A. J. Moreno, F. Sciortino, and W. Kob, Phys. Rev. Lett. **94**, 215701 (2005).
[19] W. Gotze, A. P. Singh, and T. Voigtmann, Phys. Rev. E **61**, 6934 (2000).
[20] J. Hammann, E. Vincent, V. Dupuis, M. Alba, M. Ocio, and J.-P. Bouchaud, J. Phys. Soc. Jpn. **69**, 206 (2000).
[21] M. Tarzia and M. A. Moore, Phys. Rev. E **75**, 031502 (2007).
[22] B. Berkovski, *Magnetic Fluid Handbook* (UNESCO, 2001).
[23] F. Cousin, E. Dubois, and V. Cabuil, Phys. Rev. E **68**, 021405 (2003).
[24] G. Mériguet, E. Dubois, V. Dupuis, and R. Perzynski, J. Phys.: Condens. Matter **18**, 10119 (2006).
[25] A. Robert, E. Wandersman, E. Dubois, V. Dupuis, and R. Perzynski, EPL **75**, 764 (2006).
[26] E. Hasmonay, E. Dubois, J.-C. Bacri, R. Perzynski, Y. Raikher, and V. Stepanov, Eur. Phys. J. B **5**, 859 (1998).
[27] E. Hasmonay, A. Bee, J. C. Bacri, and R. Perzynski, J. Phys. Chem. B **103**, 6421 (1999).
[28] G. Mériguet, M. Jardat, and P. Turq, J. Chem. Phys. **123**, 144915 (2005).
[29] G. Mériguet, G. Demouchy, E. Dubois, R. Perzynski, and A. Bourdon, J. Non-Equilib. Thermodyn. **32**, 271 (2007).
[30] R. Skurtveit and U. Olsson, J. Phys. Chem. **96**, 8640 (1992).
[31] K. Binder and W. Kob, *Glassy Materials and Disordered Solids: An Introduction to Their Statistical Mechanics* (World Scientific, Singapore, 2005).
[32] E. V. Colla, L. K. Chao, and M. B. Weissman, Phys. Rev. B **63**, 134107 (2001).
[33] G. H. Koenderink, H. Zhang, M. P. Lettinga, G. Nagele, and A. P. Philipse, Phys. Rev. E **64**, 022401 (2001).
[34] V. Degiorgio, R. Piazza, and R. B. Jones, Phys. Rev. E **52**, 2707 (1995).
[35] D. Parker, F. Ladieu, E. Vincent, G. Mériguet, E. Dubois, V. Dupuis, and R. Perzynski, J. Appl. Phys. **97**, 10A502 (2005).
[36] L. Berthier, G. Biroli, J.-P. Bouchaud, L. Cipelletti, D. E. Masri, D. L'Hôte, F. Ladieu, and M. Pierno, Science **310**, 1797 (2005).
[37] G. Tarjus and D. Kivelson, J. Chem. Phys. **103**, 3071 (1995).
[38] G. Biroli, arXiv:cond-mat/0504681.
[39] F. Bert, V. Dupuis, E. Vincent, J. Hammann, and J.-P. Bouchaud, Phys. Rev. Lett. **92**, 167203 (2004).
[40] W. Kob and J.-L. Barrat, Phys. Rev. Lett. **78**, 4581 (1997).
[41] J.-P. Bouchaud, V. Dupuis, J. Hammann, and E. Vincent, Phys. Rev. B **65**, 024439 (2001).